合同セッション | 合同セッション（地盤力学の理論と応用の最前線）

2026年5月17日(日) 10:35 ~ 11:50 | D会場(環境棟：5階講義室)

地盤力学の理論と応用の最前線 (2)

座長:藤澤 和謙(京都大学)

10:35 ~ 10:50

[24006] 土石流モデリングのための浅水流SPHフレームワークへの侵食および連行過程の導入（シンポジウム講演概要）

*Dolojan Nilo[1]、辻 勲平[1]、野村 怜佳[1]、寺田 賢二郎[1]、森口 周二[1] (1. 東北大学)

10:50 ~ 11:05

[24007] Binghamモデルを適用したMPS法による土石流に対するため池の減災機能の評価（シンポジウム講演概要）

*柴田 俊文[1]、絹輪 太一[1]、西村 伸一[1] (1. 岡山大学)

11:05 ~ 11:20

[24008] 3次元DEM/2次元SMAC連成解析による土砂輸送における土と流体の相互作用に関する研究 (シンポジウム講演概要)

*アフメド エムディー シャミム[1]、チョウドリー ファズルルハビブ[1]、松島 高志[1] (1. 筑波大学)

11:20 ~ 11:35

[24009] 底面粗度を有する斜面粒状体流れの個別要素法解析および極性流体理論によるモデル化（シンポジウム講演概要）

*横田 直孝[1]、岩井 裕正[1]、内藤 直人[2] (1. 京都大学、2. 豊橋技術科学大学)

11:35 ~ 11:50

[24010] 細粒分に富む熱海土石流発生源土砂のレオロジー特性評価（シンポジウム講演概要）

*ファズルルハビブ チョウドリー[1]、高志 松島[1]、猛司 小高[2] (1. 構造エネルギー工学域, 筑波大学、2. 社会基盤デザイン工学科, 名城大学)

Incorporating erosion and entrainment into a shallow water SPH framework for debris flow modeling (Proceedings of Symposium on Applied Mechanics)

Nilo Lemuel DOLOJAN, Tohoku University
Kumpei TSUJI, Tohoku University
Reika NOMURA, Tohoku University
Kenjiro TERADA, Tohoku University
Shuji MORIGUCHI, Tohoku University
E-mail: dolojan.nilo.lemuel.junio.b2@tohoku.ac.jp

Debris flows are highly destructive gravity-driven mixtures that significantly increase in volume through bed-sediment erosion and entrainment. While conventional depth-integrated Shallow Water Smoothed Particle Hydrodynamics (SWSPH) models are computationally efficient for large-scale simulations, their constant-mass assumption fundamentally contradicts the physics of entrainment. This paper introduces a framework to resolve this physical inconsistency by extending the SWSPH method to allow for variable particle mass. Validated against analytical solutions, large-scale experiments, and a real-world event, the proposed method accurately reproduces large-scale flow propagation, deposition, and mass growth.

1. Introduction

Debris flows are rapid, gravity-driven mixtures of rock, sediment, and water, whose volume increase through bed-sediment erosion and entrainment. These processes significantly increase the debris flow's destructive potential, substantially enhancing its mobility and runout distance. Depth-integrated Shallow Water Equations (SWE) solved using Smoothed Particle Hydrodynamics (SPH) provide an efficient way to simulate these events at large scales, making them valuable for hazard assessment.

Conventional shallow water SPH (SWSPH) formulations, however, enforce a constant particle mass assumption, which prevents them from representing the mass growth that occurs during erosion and entrainment. Therefore, this study introduces a method that incorporates these processes directly into the SWSPH framework, enabling more physically consistent simulations of debris flow and improving the reliability of hazard modeling.

2. Governing Equations

The physical model utilizes depth-integrated Lagrangian SWE that account for entrainment:

$$\frac{Dh}{Dt} + h\nabla \cdot \bar{\boldsymbol{u}} = E \tag{1}$$

$$\frac{D\bar{\boldsymbol{u}}}{Dt} = \boldsymbol{g} - \frac{k}{h}\nabla P - \frac{\boldsymbol{\tau}_b}{\rho h} + \frac{(\boldsymbol{u}_b - \bar{\boldsymbol{u}})}{h}E \tag{2}$$

where D/Dt is the total material deriative, h is the flow depth, $\bar{\boldsymbol{u}}$ is the depth averaged velocity vector, k is the lateral earth pressure coefficient, $P = \frac{1}{2}gh^2$ is the pressure, g is the acceleration due to gravity, ρ is the density and $\boldsymbol{\tau}_b$ is the bed shear stress vector.

The framework incorporates a lateral earth pressure coefficient to address anisotropic pressure distributions common in granular-fluid flows. This coefficient adopts values derived from Rankine Theory depending on whether the flow is expanding (active state) or compressing (passive state):

$$k_a = \frac{1 - \sin\phi}{1 + \sin\phi} \tag{3}$$

$$k_p = \frac{1 + \sin\phi}{1 - \sin\phi} \tag{4}$$

where ϕ is the internal friction angle, and k_a, k_p refers to the active or passive state of the flow, respectively.

Flow resistance is captured through a composite rheological model combining Manning's turbulent friction and Coulomb's frictional model:

$$\tau_{bt} = \frac{\bar{\rho} g_z n^2 \bar{u}\sqrt{\bar{u}^2 + \bar{v}^2}}{h^{1/3}} \tag{5}$$

$$\tau_{bf} = \bar{\rho} g_z h \tan\phi \tag{6}$$

$$\tau_b = \tau_{bt} + \tau_{bf} \tag{7}$$

where n is the Manning's friction coefficient, α is the slope gradient, and ϕ is the internal friction angle of the material.

Finally, The entrainment rate is calculated using a physics-based model based on a momentum balance at the interface between the moving flow and the static bed:

$$E = -\frac{\partial z_b}{\partial t} = \frac{\tau_b - \tau_{yield}}{\bar{\rho}(|\boldsymbol{u}_b| - |\boldsymbol{u}_{bed}|)} \tag{8}$$

where $\tau_b, \boldsymbol{u}_b = [u_b, v_b]^T$ are the stress and velocity at the bottom of the moving flow layer, while $\tau_{yield}, \boldsymbol{u}_{bed} = [u_{bed}, v_{bed}]^T$ are the stress and velocity at the surface of the erodible bed layer. The flow basal shear stress τ_b is the combined turbulent and frictional model defined for the debris flow (Eq. 7), while the yield stress τ_{yield} is defined using the Mohr-Coulomb failure criterion for the erodible layer. Erosion initiates when the basal shear stress of the flow exceeds the yield stress of the bed.

3. SPH discretization

The above equations are solved using the mesh-free Lagrangian SPH approach. discretizing the above equations for a particle i can be written as:

$$h_i = \sum_{j=1}^{N} V_j W_{ij} + E_i \Delta t \tag{9}$$

$$\frac{D\bar{\boldsymbol{u}}_i}{Dt} = \boldsymbol{g}_i - k\sum_{j=1}^{N} V_j \left(\frac{P_i + P_j}{h_i h_j} + \Pi_{ij}\right)\nabla W_{ij} - \frac{\boldsymbol{\tau_{bi}}}{\rho h_i} + \frac{(\boldsymbol{u}_{bi} - \bar{\boldsymbol{u}}_i)E_i}{h_i} \tag{10}$$

As discussed earlier, the constant mass assumption of conventional SPH prevents the direct incorporation of entrainment. As seen in Eq. (9), the flow depth h_i is calculated using the standard SPH summation, which is subsequently increased by adding entrainment. This creates a non-physical state where the flow height artificially increases while the particle mass and volume remain unchanged, potentially violating mass and momentum conservation.

A more consistent approach is to adopt a variable-mass formulation. Rather than artificially increasing particle height, the particle volume is updated according to the entrained volume, computed as the entrained height $E_i \Delta t$ multiplied by the representative particle area A:

$$V_i^{n+1} = V_i^n + E_i^n A_i^n \Delta t = V_i^n + E_i^n \frac{V_i^n}{h_i^n} \Delta t \tag{11}$$

The flow height then evolves naturally through the conservative, summation-based continuity equation, and the entrained volume is consistently incorporated into the momentum equation.

4. Results

4.1. Analytical dam break

The framework was validated against a one-dimensional analytical solution for a dry bed granular dam break[1]. Simulated over varying bed friction angles corresponding to 0° (Case A), 15° (Case B), and 30° (Case D), the model accurately captured the propagation of the rarefaction wave and the location of the flow front.

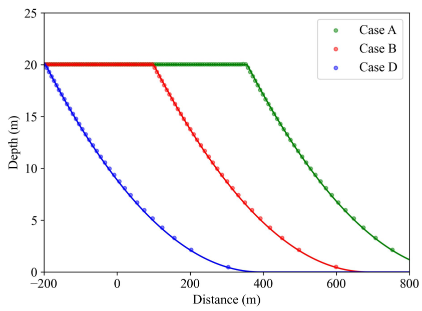

Fig. 1 Comparison of numerical and analytical results showing the effect of varying bed friction angles on the flow profiles at t = 15 s

4.2. USGS debris flow experiment

The model simulated a 6 m^3 debris flow released down a 95 m long flume. Baseline rheological parameters were calibrated using a non-erodible bed experiment, establishing a Manning's coefficient of 0.03 and an internal friction angle of 8°. Simulations incorporating a 0.12 m thick erodible bed successfully replicated the experimentally observed sustained flow front velocities, arrival times, and peak flow heights.

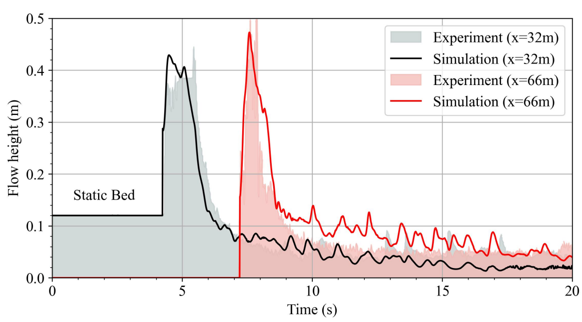

Fig. 2 Good agreement between the observed and simulated debris flow heights at different obsertvations points along the flume for the erodible bed experiment

The conservative nature of the variable mass SWSPH is illustrated by tracking the cumulative volume changes of the system. As the flow front propagates, the total debris flow volume increases significantly from an initial 5.84 m^3 to a final volume of approximately 15.96 m^3. This total entrained volume of 10.12 m^3 directly corresponds to the material lost from the erodible bed, demonstrating the strict global mass conservation achieved by the framework.

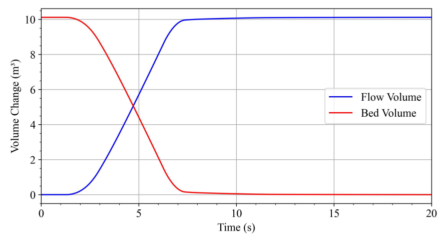

Fig. 3 Cumulative volume change for both the debris flow and the erodible bed

4.3. Marumori debris flow event

To demonstrate regional-scale applicability, the model simulated a 2019 debris flow in Marumori, Japan, utilizing a 1 m resolution digital elevation model. The initial failure volume of 3,660 m^3 expanded to 4,930 m^3 through bed entrainment. The simulated erosion patterns and final depositional geometry were spatially consistent with post-disaster field observations.

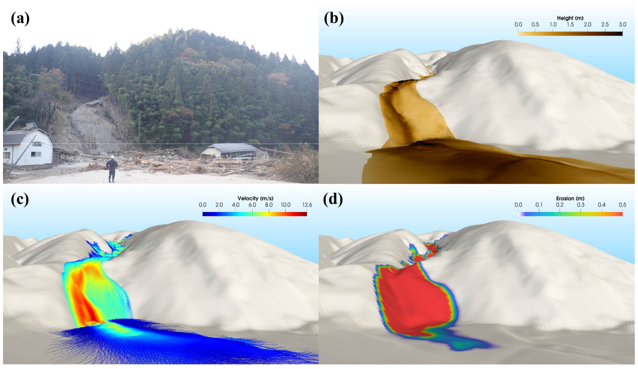

Fig. 4 Marumori debris-flow comparison: (a) Post-event photo of the eroded runout path. (b) Simulated flow height at t=30 s. (c) Simulated velocity paths from t=0-30 s. (d) Final erosion depth at t=60 s

5. Conclusion

Conventional SWSPH methods are fundamentally limited by a constant-mass assumption that fails to physically account for the mass growth of debris flows due to bed erosion and entrainment. By introducing a variable-mass SWSPH formulation that dynamically updates particle volume based on entrained height, this study resolves these inconsistencies and ensures a rigorous coupling between mass, geometry, and momentum. Validation against analytical solutions, USGS flume experiments, and actual debris flows confirms that this approach accurately captures flow heights, arrival times, and mass growth of debris flows.

References

1) Faccanoni, G., et al, (2013). Exact solution for granular flows. IJNAMG.
2) Iverson, R. M., et al, (2011). Positive feedback and momentum growth during debris-flow entrainment of wet bed sediment. Nat Geosci.

Bingham モデルを適用した MPS 法による土石流に対するため池の減災機能の評価（シンポジウム講演概要）

Evaluation of Disaster Mitigation Function of Reservoir against Debris Flow Using MPS Method with Bingham Fluid Model (Proceedings of Symposium on Applied Mechanics)

絹輪　太一（岡山大）　　柴田　俊文（岡山大）　　西村　伸一（岡山大）
Taichi KINUWA, Okayama University
Toshifumi SHIBATA, Okayama University
Shin-ichi NISHIMURA, Okayama University
E-mail: tshibata@cc.okayama-u.ac.jp

In recent years, the frequency of heavy rainfall disasters has shown an increasing trend due to climate change, which is considered to be caused by global warming. Under such circumstances, there have been several reported cases in which debris flows generated during disasters are trapped within reservoirs, thereby providing a disaster mitigation function for downstream areas. However, the behavior of debris flows entering reservoirs and their mitigation effects have not yet been sufficiently clarified. In this paper, the Bingham model is incorporated into the MPS method to evaluate and examine the disaster mitigation function of reservoirs.

１．はじめに

近年，地球温暖化に起因すると考えられる急激な気候変動の影響により，局地的かつ短時間の豪雨の発生頻度が急増している．これに伴い，土砂災害の発生件数は増加傾向を示しており，土石流は周辺地域の被害拡大に大きな影響を及ぼす可能性がある．土石流がため池流入した場合，貯水池内での堆積や水位上昇，さらには越流や堤体破壊を引き起こすことが懸念され，下流域に二次的な被害をもたらす危険性がある．その一方で，土石流が流入したため池が貯水位池内で土砂を受け止め，下流に対して減災機能を発揮している事例も散見される．しかし，土石流がため池に流入した際の挙動把握や，堤体に作用する力学的影響については，十分に解明されていないのが実情である．

本論文では，MPS（Moving Particle Semi-implicit）法を用い，土石流に対して Bingham 流体でモデル化して，1)土石流の物性がため池堤体・越流量に作用する影響，2)ため池堤体の土石流捕捉率，の 2 つの観点からため池の減災機能について検討する．

２．MPS 法

MPS 法は越塚 [1]によって提案された粒子法で，その特徴は，支配方程式の勾配，発散，ラプラシアンといった微分演算子を粒子間の相互作用モデルを使って離散化する点である．この手法では，Navier-stokes 方程式に半陰的アルゴリズムを適用し，粒子の圧力勾配や速度を計算する．ラグランジュ法に基づき，粒子が流れに沿って移動するため，対流項を考慮する必要がないという特徴がある．そのため，有限要素法等と比較すると，自由表面や大変形などの変形の大きい物理現象を解く際に非常に優れているという利点がある．

本論文では，境界部にポリゴン壁モデル [2]を採用し，土石流の挙動を再現するために，非ニュートン流体の一つである Bingham モデル [3]を適用した．Bingham 流体は，降伏値を持ち，せん断応力が一定の限界値に達するまでは流動せず，せん断応力が降伏応力以上になると流動を開始するという特徴がある．式(1)に Bingham 流体の粘度を表す式を示す．

$$\eta = \frac{\tau_B}{\dot{\gamma}} + \eta_B \qquad (1)$$

ここで，τ_Bは降伏応力（Pa），$\dot{\gamma}$はせん断速度（s^{-1}），η_Bは降伏後の粘度（Pa·s）である．

３．土石流の物性がため池堤体・越流量に作用する影響

Bingham 流体の物性を表す降伏応力τ_B，降伏後の粘度η_Bを変化させ，土砂濃度および，土砂密度を算出する．そして，土砂濃度とため池堤体・越流量に作用する影響を検討する．ここで Fig. 1 に示す解析モデルおよび Table 1 の解析諸元を用い，降伏応力τ_Bを 3，15，60Pa の 3 ケース，降伏後の粘度η_Bを，0.01，0.3，10Pa·s の 3 ケースとした計 9 ケースについて解析を実施した．Fig. 2 にτ_B=60Pa，η_B=0.3Pa·s とした際の，ため池に流入する土石流の解析結果を示す．

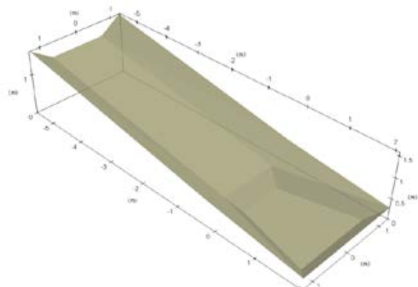

Fig.1 Numerical model.

Table 1 Simulation parameters.

Particle distance (m)	0.04
Time increment (s)	0.00025
Density of water (kg/m³)	1000
Plastic viscosity of water (Pa·s)	0.000001
Courant number	0.1
Parameter for collision condition	1

Fig. 2 Simulation results of the debris flow with τ=60 Pa and η=0.3 Pa·s.

Fig. 3 は，土砂濃度とため池堤体に作用する荷重に関し，降伏後の粘度η_Bの値毎に示したものである．η_B=10Pa·s の際は，降伏後の粘度が高いため土石流がため池堤体まで届かず，作用荷重が小さくなったいることが確認できる．Fig. 4 に土砂濃度と越流量の関係を示す．図より，土砂濃度の増加に伴い，越流量が減少傾向を示していることがわかる．

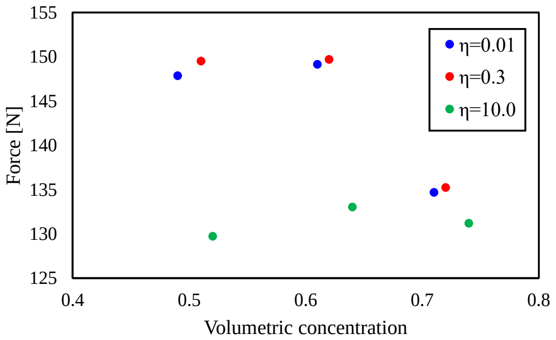

Fig. 3 Relationship between force and volumetric concentration.

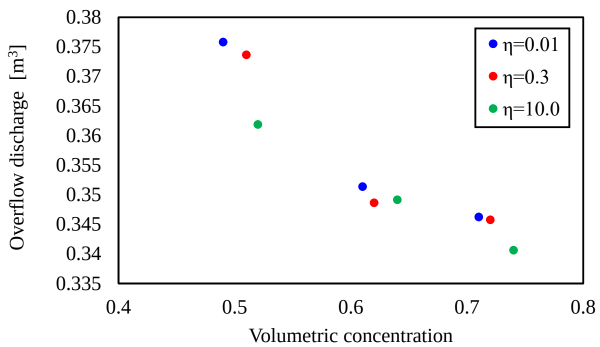

Fig. 4 Relationship between overflow discharge and volumetric concentration.

４．ため池堤体の土石流捕捉率の評価

降伏応力τ，降伏後の粘度η，ため池に至る勾配θ，貯水位 h を因子，越流量を応答とし，MPS 法によって得られた解析結果を用いて応答曲面法を適用する．貯水および土石流の両者を含む全体の越流量を Q_{OV}，土石流のみの越流量を Q_{OV}^{df} とすると，それぞれ式(2)および式(3)が得られた．

$$Q_{OV} = -0.00122\tau - 0.00655\eta + 0.009313\theta + 0.009314h + 0.019989 \quad (2)$$

$$Q_{OV}^{df} = -0.00168\tau - 0.00898\eta + 0.01028\theta + 0.002387h + 0.126732 \quad (3)$$

ここで，式(2)，式(3)の決定係数はそれぞれ 0.981 および 0.988 となった．また，流下する土石流をため池が堰き止める指標を捕捉率とし，貯水と土石流の両者に対する捕捉率を C_{cap}，土石流の捕捉率を C_{cap}^{df} とすると，C_{cap} および C_{cap}^{df} は，式(4)および式(5)で表すことができる．

$$C_{cap} = 1 - \frac{Q_{OV}}{Q_{in}}, \quad C_{cap}^{df} = 1 - \frac{Q_{OV}^{df}}{Q_{in}} \quad (4),(5)$$

ここで，Q_{in} は土砂流入量である．

次に，土石流の物性を確率分布で表し，式(2)と(3)から越流量を求める．勾配θは 10°で固定し，貯水位は 0.11，0.18 および 0.25m の 3 ケースについて算出する．得られた結果から捕捉率を算定し，その分布特性を用いて捕捉率を評価する．Fig. 5(a), (b)に土石流のみと貯水と土石流全体のそれぞれの捕捉率を示す．いずれのケースも貯水位が高いほど土石流の越流量は大きくなっていることが確認できる．

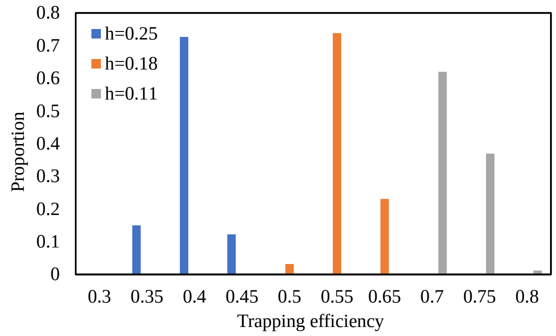

(a) Debris flow

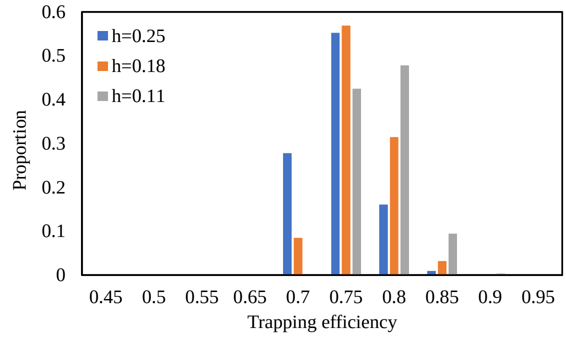

(b) Debris flow and water

Fig. 5 Distribution of trapping efficiency at different water level.

５．おわりに

土石流のモデルに Bingham 流体を採用し，MPS 法で解析を行った．ため池の土石流に対する減災機能について，土石流の物性により変化する作用荷重，越流量を評価することができた．また，捕捉率について，貯水位が低い条件ほど土石流の捕捉率が高くなる傾向が示された．

参考文献

1) 越塚誠一：計算力学レクチャーシリーズ 5 粒子法，丸善出版, 2005.
2) 原田隆宏，越塚誠一，島崎克教：MPS 法における壁境界計算モデルの改良，日本計算工学会論文集，Vol. 2008, P 20080006, 2008.
3) 五十里洋行，後藤仁志，新井智之：粒子法型非ニュートン流体モデルによる地滑り津波解析，土木学会論文集 B2(海岸工学), Vol.68, No.2, p. I_66-I_70, 2012.

Coupled 3D-DEM/2D-SMAC Analysis of Soil-Fluid Interactions in Sediment Transport (Proceedings of Symposium on Applied Mechanics)

Md Shamim AHMED, University of Tsukuba
Fazlul Habib CHOWDHURY, University of Tsukuba
Takashi MATSUSHIMA, University of Tsukuba
E-mail: msahmed.ce@gmail.com

This study examines sediment transport mechanics using a coupled three-dimensional Discrete Element Method (DEM) and two-dimensional Simplified Marker and Cell (SMAC) numerical framework. Pressure-driven flow over a granular bed of uniform spherical particles of 2 mm diameter is simulated at varying pressure gradients per unit density (g_f = 200–1000 cm/s²) and computational domain sizes. The resulting fluid velocity and particle concentration profiles are analyzed and compared with established sediment transport theories to evaluate the model's capability to describe the fundamental mechanics of sediment transport at the particle scale.

1 Introduction

Debris flows are a critical concern in geotechnical engineering, and predicting these hazards remains challenging due to the complex soil–fluid interactions during erosion and sedimentation. The erosion, transport, and deposition of sediment are largely governed by the balance between gravitational settling and turbulent drag, as reflected in the vertical distribution of particle concentration. This distribution can be described by the Rouse equation (Rouse[1]), which characterizes the transport regime by Rouse number Z.

While these theoretical and experiential approaches provide a macroscopic framework, understanding the microscale mechanics of soil-fluid interactions requires particle-scale computational techniques. To this end, numerical modeling such as the discrete element method (DEM) coupled with computational fluid dynamics (CFD) has become an increasingly practical tool for studying soil-fluid interactions at the particle scale (Nguyen and Indraratna[2], Ramezanzad et al.[3]). In coupled models, DEM tracks the behavior of individual soil particles within granular assemblies, accounting for their mutual interactions and external forces, while CFD simulates the fluid field's response.

In this study, a Fortran-based computational approach that couples a three-dimensional Discrete Element Method (3D-DEM) with a two-dimensional Simplified Marker and Cell (2D-SMAC) numerical framework is employed to simulate pressure-driven flow over a sediment bed at varying flow intensities. Simulation results are systematically evaluated against established erosion and sedimentation theories to examine whether the model can predict the settling–diffusion equilibrium. By integrating the microscale particle-level insights with theoretical sediment transport frameworks, this research contributes to a more comprehensive understanding of soil–fluid interactions in natural erosion and sedimentation processes.

2 Numerical Method

2.1. 3D-DEM/2D-SMAC Coupling

The coupled model integrates a 3D-DEM for granular particle mechanics with a 2D-SMAC fluid solver through a two-way momentum-exchange scheme. The DEM (Cundall and Strack[4]) tracks the motion and interaction of individual particles, incorporating the fluid drag using Newton's law, as described by the following governing equations:

$$m_i \ddot{x}_i = \sum_j F_{ij}^c + m_i g\left(1 - \frac{\rho_f}{\rho_s}\right) + F_i^{drag} \quad (1)$$

Where m_i is the particle mass, $\ddot{x}_i$ is the acceleration, F_{ij}^c is the contact force, g is the gravitational acceleration, ρ_f and ρ_s are the fluid and solid densities, and F_i^{drag} is the fluid drag force. The contact force is calculated using a linear spring–dashpot model (Fig. 1), and the fluid–particle interaction is modeled using the Di Felice (1994) drag correlation (Di Felice[5]).

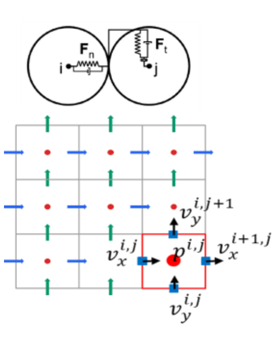

Fig. 1 DEM and SMAC

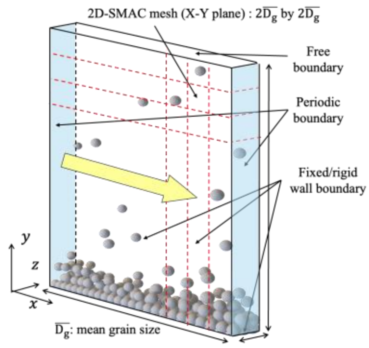

Fig. 2 Model schematic

The fluid phase is solved on a two-dimensional staggered grid (Fig. 1) using the SMAC method. The governing equations are the continuity equation and the simplified momentum equation for the fluid phase:

$$\frac{\partial \varepsilon}{\partial t} + \frac{\partial(\varepsilon v_i)}{\partial x_i} = 0 \quad (2)$$

$$\frac{\partial v_i}{\partial t} + v_j \frac{\partial v_i}{\partial x_j} = -\frac{1}{\rho_f}\frac{\partial p}{\partial x_i} + \nu \nabla^2 v_i + \frac{F_{pi}}{\rho_f \varepsilon} + g_f \quad (3)$$

Where ε is the local porosity, v_i is the fluid velocity component, ρ_f is the fluid density, p is the pressure, ν is the kinematic viscosity, g_f is the pressure gradient per unit density, and $\frac{F_{pi}}{\rho_f \varepsilon}$ is the grain–fluid interaction force per unit mass.

2.2. Simulation Setup

Simulations are performed across multiple computational domain sizes with streamwise lengths L = 8, 12, 16, and 32 cm, a fixed vertical height H = 10 cm, and a spanwise width of 1 cm, containing uniform-sized spherical particles (diameter D_g = 2 mm and density ρ_s = 2.5 g/cm³) maintaining the same solid volume fraction at the sediment bed. The fluid has density ρ_f = 1.0 g/cm³ and kinematic viscosity ν = 1.0 × 10⁻² cm²/s. Fluid flow is driven by a pressure gradient per unit fluid density, g_f = 200, 400, 600, 800, and 1000 cm/s². Boundary conditions are shown in Fig. 2, periodic in x and z (streamwise and spanwise), with a rigid no-slip bottom wall and a free surface (zero shear stress) at the top. Fig. 3 shows a snapshot of the particle distribution in the 32x10x1 cm domain at g_f = 600 cm/s², illustrating the particle suspension under stronger flow. Each simulation runs for 16 s, with results time-averaged over t = 14–16 s after the steady state is reached.

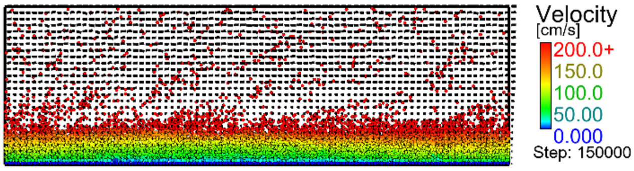

Fig. 3 32x10x1 cm, n = 8000, g_f = 600 cm/s^2

3 Results and Discussion

3.1. Velocity Profile

Fig. 4 shows the time-averaged horizontal fluid velocity profiles for varying streamwise domain sizes (L) as a function of normalized height y/H for g_f = 200–800 cm/s². The profiles show the expected flow structure over a sediment bed, near-zero seepage velocity within the packed bed (y/H < 0.2), a transition zone at the bed–fluid interface where the velocity increases rapidly and reaches a maximum in the suspension zone near the free surface. The maximum velocity ranges from ~600 cm/s at g_f = 200 to ~1400 cm/s at g_f = 800 cm/s². Also, the obtained velocity profiles show a less significant effect of L if the flow is homogeneous. The flow structure is consistent with experimental results reported by Itoh and Egashira[6].

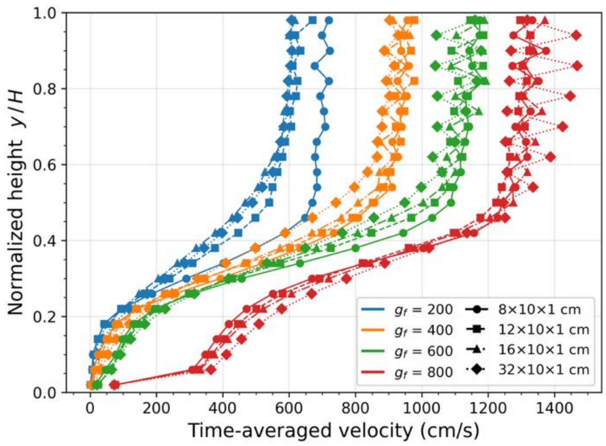

Fig. 4: Time-averaged velocity profiles

3.2. Concentration Profiles and Rouse Fitting

The time-averaged concentration profiles are shown in Fig. 5 on a semi-logarithmic scale as a function of normalized height y/H. The concentration remains nearly constant within the packed bed, decreases above the bed–fluid interface. Higher g_f values result in greater particle suspension into the upper flow region due to the stronger driving forces.

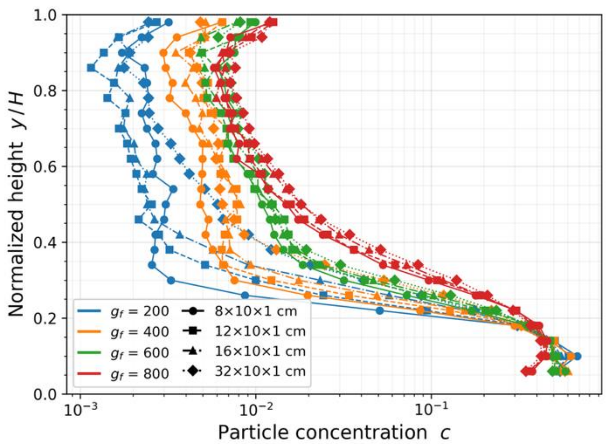

Fig. 5: Particle concentration profiles

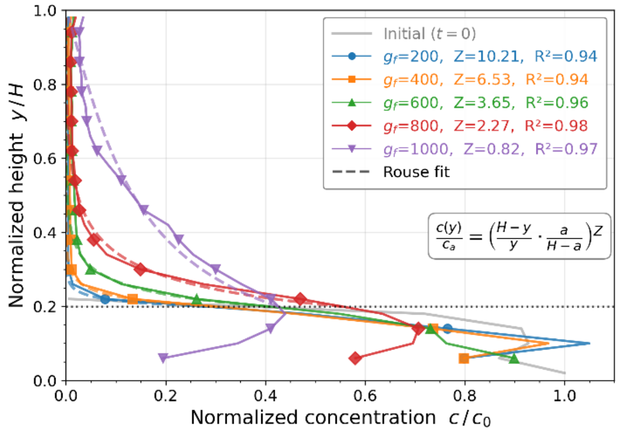

Fig. 6: Concentration profiles and Rouse fitting (8x10x1 cm)

The Rouse equation:

$$\frac{c(y)}{c_a} = \left(\frac{H-y}{y} \cdot \frac{a}{H-a}\right)^Z \qquad (4)$$

where a is the reference height (considered at y/H= 0.2), $c(y)$ is the concentration at each vertical position y, c_a is the concentration at y= a, and Z is the Rouse number. This equation is fitted to the suspension zone shown in Fig. 6 for g_f = 200–1000 cm/s² in the 8x10x1 cm domain. Notably, the fitted Z values classify the flow conditions into bed load (Z = 10.21, 6.53, 3.65 at g_f = 200, 400, 600 cm/s²), 50% suspended (Z = 2.27 at g_f = 800 cm/s²), and fully suspended (Z = 0.82 at g_f = 1000 cm/s²), with Z decreasing as flow intensity increases. Furthermore, this classification is also consistent with the visual particle distribution shown in Fig. 3.

4 Conclusion

This study demonstrated the capability of the coupled model to predict sediment transport under pressure-driven flow. The simulated fluid velocity profiles show an expected flow structure consistent with previous experimental results. The particle concentration profiles show the expected transition from the bed load to suspended load for different flow intensities and are consistent with the Rouse model. These results confirm that the coupled 3D-DEM/2D-SMAC numerical model can resolve the fundamental behavior of both erosion and particle suspension at the grain scale. The effects of domain size and particle size distribution will be evaluated in a future study.

References

1) Rouse, H.: Modern conceptions of the mechanics of fluid turbulence, Trans. ASCE, 102, 463-505, 1937.
2) Nguyen, T. T., and Indraratna, B.: Fluidization of soil under increasing seepage flow: an energy perspective through CFD-DEM coupling. Granular Matter, 24(3), 80, 2022.
3) Ramezanzad, A., Jaradat, K., and Abdelaziz, S.: Coupled CFD-DEM simulations: A review of applications and modeling limitations. IFCEE 2024, 216-226, 2024.
4) Cundall, P. A., and Strack, O. D.: A discrete numerical model for granular assemblies. Geotechnique, 29(1), 47-65, 1979.
5) Di Felice, R.: The voidage function for fluid-particle interaction systems. Int. J. Multiphase Flow, 20(1), 153-159, 1994.
6) Itoh, T., & Egashira, S.: Critical condition of sediment entrainment by sediment-water mixture flow. Proc. of the 5th IAHR Symp. RCEM, Vol. 1. CRC Press, 2019.

底面粗度を有する斜面粒状体流れの個別要素法解析および極性流体理論によるモデル化（シンポジウム講演概要）

Discrete Element Method Analysis and Micropolar Fluid Modeling of Granular Flow Down an Inclined Plane with Basal Roughness (Proceedings of Symposium on Applied Mechanics)

横田　直孝（京都大・都市社会工学専攻）　　岩井　裕正（京都大・都市社会工学専攻）
内藤　直人（豊橋技科大・建築 都市システム学系）
Naotaka YOKOTA, Kyoto University
Hiromasa IWAI, Kyoto University
Naoto NAITO, Toyohashi University of Technology
E-mail: yokota.naotaka.52y@st.kyoto-u.ac.jp

A granular flow model based on micropolar fluid theory formulated by Kano was examined under basal roughness conditions. DEM simulations of unidirectional granular flow down an inclined plane were conducted to determine model parameters. The results show that the steady flow can be reproduced by applying a Dirichlet boundary condition for rough surfaces and a Navier slip boundary condition for smooth surfaces.

1. はじめに

土石流やがけ崩れをはじめとする粒状体流れは，構成粒子が大きく流れに対して粒子同士の相互作用の影響が無視できない．連続体理論である極性流体理論 (Micropolar Fluid Theory)[1] を用いた粒状体の流動モデルは，巨視的な流れと粒子の微視的な運動を結びつけて記述できる．既往の研究においては，個別要素法（以下，DEM と記す）[2] を用いた粒状体流れの数値実験と比較して，流速分布を表現できた一方で，底面粗度のない極端に理想化された条件での検討に限られていた．実際の斜面流れは，崩壊面に土粒子や礫が存在し，底面は粗度を有するため，工学的な議論には底面境界条件の検討が必要となる．

そこで本研究では，加納ら[3] の極性流体理論に基づく粒状体流動モデルの工学的利用に向けて，DEM を用いて底面粗度を有する斜面流れの解析を行った．得られた結果から粒状体流れを特徴づけるパラメータを決定し，極性流体理論モデルに適用した．また，底面境界条件としてディリクレ境界条件および Navier すべり境界条件を導入した．

2. 極性流体理論による粒状体流れの支配方程式

加納ら[3] が提案した極性流体理論に基づく粒状体流れの連続式，運動方程式，角運動方程式は次式で与えられる．以下では，添え字の総和規約を用いる．

$$\frac{\mathrm{d}\rho}{\mathrm{d}t} + \rho\frac{\partial v^k}{\partial x_k} = 0 \tag{1}$$

$$\rho\frac{\mathrm{d}v^i}{\mathrm{d}t} = \frac{\partial \sigma^{ji}}{\partial x_j} + \rho b^i \tag{2}$$

$$\frac{2}{5}\rho a^2\frac{\mathrm{d}\omega_{ji}}{\mathrm{d}t} = \frac{\partial \mu^{kji}}{\partial x_k} + 2\sigma^{[ji]} \tag{3}$$

ここに，ρ は粒状体流れの密度，v^i は速度，ω_{ji} は回転速度を表す．σ_{ji} は通常の応力であり，μ^{kji} は物体を回転させる作用を持つ偶応力を表す．b^i は単位質量当たりの外力である．また，$\sigma^{[ji]}$ は添え字の反対称化を表し，$\sigma^{[ji]} = (1/2)\left(\sigma^{ji} - \sigma^{ij}\right)$ である．

この支配方程式を，Fig.1 のような傾斜角度 θ の斜面上一方向流れに適用すると，次式のようになる．

$$\rho\frac{\mathrm{d}u}{\mathrm{d}t} = C(\rho)\frac{\partial}{\partial y}\left\{\hat{\omega}\left(\frac{2}{5}\frac{\partial u}{\partial y} + \frac{1}{2}\omega\right)\right\} + \rho g \sin\theta \tag{4}$$

$$\rho\frac{\mathrm{d}\omega}{\mathrm{d}t} = \frac{5C(\rho)}{2a^2}\left\{-\hat{\omega}\left(\frac{1}{2}\frac{\partial u}{\partial y} + \omega\right) + \frac{a^2}{10}\frac{\partial}{\partial y}\left(\hat{\omega}\frac{\partial \omega}{\partial y}\right)\right\} \tag{5}$$

$$\hat{\omega} = \sqrt{\left(\frac{1}{2}\frac{\partial u}{\partial y} + \omega\right)^2 + \frac{3}{20}\left(\frac{\partial u}{\partial y}\right)^2 + \frac{2a^2}{5}\left(\frac{\partial \omega}{\partial y}\right)^2} \tag{6}$$

$$C(\rho) = \frac{2\sqrt{6}}{15}\frac{\mu e T a^3 \rho}{r - r_0} + \frac{\sqrt{10}}{50}\frac{T\sqrt{T}a^3\rho}{r - r_0}\frac{e(1-e)^2}{(1+e)\sin\zeta} \tag{7}$$

u は流下方向の粒子速度，ω は粒子の回転速度で，逆回転を正としている．また T はエネルギー比であり，平均流速からの各粒子速度ずれである微視的偏差速度により定まる微視的な運動エネルギー E_k と粒子の回転エネルギー E_r の比であり，$T = E_k/E_r$ で定義される．

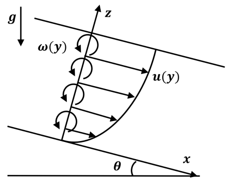

Fig. 1　Slope granular flow

3. 粒状体流れ解析条件

斜面上一方向の粒状体流れの一例として，傾斜角度 25[°] の斜面における単一粒子から構成される粒状体流れを対象とした．粒子半径 a を 0.010[m]，粒子密度は 2.65×10^3[kg/m^3]，粒子の反発係数 e を 0.10，動摩擦係数 μ を 1.00 とした．粒子は Fig.2 に示すほぼ球形な多面体であり，回転抵抗は数値としては与えず，粒子形状に起因する回転抵抗のみを考慮した．流動前の粒状体のかさ密度 ρ_0 は 1.515×10^3[kg/m^3]，層厚 h は 0.3[m] であった．DEM 解析には，Ansys 社の DEM パッケージソフトウエアである Rocky を用い，周期境界条件で解析を実施した．初期状態は粒状体が静止した状態とし，流動速度が定常になるまで計算を実施した．

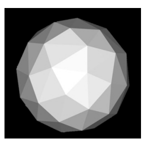

Fig. 2　Particle model

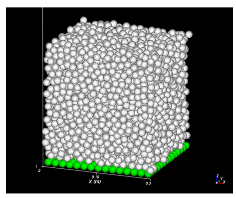

Fig. 3　DEM Slope flow

4. 境界条件

底面境界条件として，粗面条件と滑面条件の 2 ケースを検討した．DEM 解析では，滑面条件では底面の動摩擦係数を 1.00 とし，粗面条件では Fig.3 に示すように底面に流動粒子と同じ粒子を固定配置した．固定粒子は流動せず，回転も拘束されている．極性流体理論を用いた流動モデルでは，粗面条件について流動粒子と同じ粒子が固定されていることを考慮し，$u(0) = 0$，$\omega(0) = 0$ のディリクレ境界条件を課した．一方，滑面条件については，Wang らの Navier すべり境界条件[4] を用いた．Wang らは DEM 解析に基づき，底面すべり速度 u_b が底面のせん断速度 $\dot{\gamma}_b$ に比例し，すべり長さ l_s，粒径 d を用いて $u_b = l_s\dot{\gamma}_b d$ と表されることを示した．本研究では，この条件を極性流体理論を用いた流動モデルに適用した．回転速度については，滑面は回転を妨げる抵抗が働かないと仮定し，$\partial\omega(0)/\partial y = 0$ を用いた．$y = h$ の自由表面境界では，DEM 解析と同様に拘束のない自由境界と仮定した．極性流体理論のモデルではせん断応力が 0 となる条件から $\partial u(h)/\partial y = -5\omega/4$ を与え，また回転に対する抵抗がないとして $\partial\omega(h)/\partial y = 0$ を課した．

5. エネルギー比 T の決定方法

粒状体流れは，粒子運動の集合体であり，定常状態において平均値を取っても粒子乱れの影響により一定値とはならない．既往研究[5] では，定常状態のある瞬間における議論に留まり，粒子乱れを考慮した代表値の取得方法については言及されていない．一方で，エネルギー比 T は分母に粒子の回転速度エネルギー E_r を持つため，回転速度がほぼ 0 となる粒子が存在すると極端に大きな値を取る．そこで，Fig.4 のようにエネルギー比 T の累積分布を用いて評価を行い，極端に値の大きな値を除外した．本研究では，T を小さい値から累積した 96% 分位の値を代表値として採用した．その結果，底面境界が滑面の場合，$T = 299.4$，粗度がある場合は $T = 364.4$ となった．

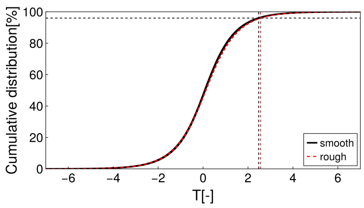

Fig. 4 Cumulative distribution of T

6. DEM 解析および極性流体理論を用いた流動モデルの数値計算結果

2 通りの境界条件について，DEM 解析を実施し，得られた諸パラメータを用いて極性流体理論を用いた流動モデルの数値計算を行った．底面が粗度条件での結果を Fig.5 と Fig.6 に，滑面条件の結果を Fig.7 と Fig.8 に示す．

DEM 解析について，底面境界に粗度がある条件では，底面付近の粒子はほとんど流下方向に速度を持たなかった一方で，底面が滑面の条件では，底面境界付近で 3.0[m/s] 程度の粒子速度を持った．しかしながら，底面から約 0.1m 以上の高さにおける速度分布は，底面境界条件によらず類似した形状となった．これらの結果から，底面近傍には粒子約 5 個分の厚さをもつ領域が境界条件の影響を受け，流れの最大速度の大きさを決定する要因となっていると考えられる．加えて本解析では，粒子の回転抵抗として多面体形状に起因する抵抗のみを考慮しているため，滑面では粒子の回転が卓越しやすく，回転する粒子の上を滑るように粒子速度が増大した可能性が考えられる．したがって，滑面においては Navier すべり境界を適用し，連続体モデルにおいても底面すべりを適切に表現する必要がある．

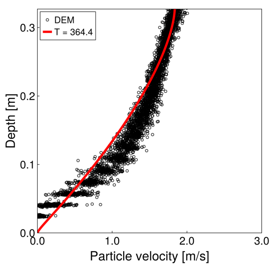

Fig. 5 Particle velocity

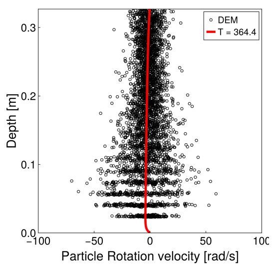

Fig. 6 Rotation velocity

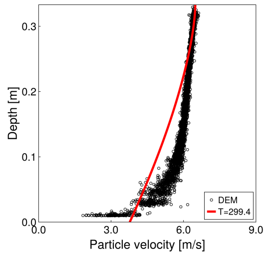

Fig. 7 Particle velocity

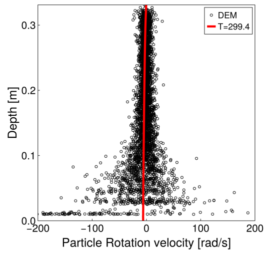

Fig. 8 Rotation velocity

極性流体理論に基づく流動モデルでは，粗面での速度分布および回転速度分布について，DEM 解析結果と良好な一致が確認できた．一方で底面が滑面の場合，底面から 0.1〜0.2m 付近において速度分布にずれが生じた．これは，滑面では底面近傍の回転速度が大きく，その増大が速度分布の形状に影響を与えたためと考えられる．

7. 結論

底面境界の異なる 2 通りの斜面上一方向の粒状体流れについて，3 次元 DEM 解析と極性流体理論を用いたモデルとの比較を通じて検証を行った．極性流体理論に基づく粒状体の流動モデルについては，底面境界条件として Navier すべり境界条件とディリクレ境界条件を導入した．その結果，得られた知見を以下に示す．

- DEM 解析より，底面境界の影響は底面から粒子約 5 個分の厚さの領域に現れることが確認された．
- 極性流体理論モデルでは，粗面にディリクレ境界条件，滑面に Navier すべり境界条件を適用することで，いずれの場合も定常状態を良好に再現できた．

今後は，2 次元流れへ拡張して数値計算を行っていく．

参考文献

1) A Cemal Eringen. Theory of micropolar fluids. *Journal of mathematics and Mechanics*, pp. 1–18, 1966.
2) P.A. Cundall and O.D.L. Strack. A discrete model for granular assemblies. *Geotechnique*, Vol. 29, No. 1, pp. 47–65, 1979.
3) 加納純也, 下坂厚子, 日高重助. 流動粒子群の構成関係に関する一考察. 粉体工学会誌, Vol. 33, No. 2, pp. 95–101, 1996.
4) Teng Wang, Lu Jing, CY Kwok, Yuri D Sobral, Thomas Weinhart, and Anthony R Thornton. Basal layer of granular flow down smooth and rough inclines: kinematics, slip laws and rheology. *Journal of Fluid Mechanics*, Vol. 1025, p. A27, 2025.
5) 横田直孝, 岩井裕正, 内藤直人. 極性流体理論および個別要素法解析に基づいた粒状体流れの定常状態の数値解析. 土木学会論文集, Vol. 82, No. 15, pp. 25–15025, 2026.

Rheological Characterization of Fines-Enriched Atami Debris-Flow Source Material (Proceedings of Symposium on Applied Mechanics)

Fazlul Habib CHOWDHURY, University of Tsukuba
Takashi MATSUSHIMA, University of Tsukuba
Takeshi KODAKA, Meijo University
E-mail: chowdhury.fazlul.fn@u.tsukuba.ac.jp

The rheological behavior of debris-flow source materials is influenced by solid concentration and fines content, yet laboratory-constrained parameters remain limited for field-relevant conditions. In this study Rotational viscometry was conducted on fines-enriched sand–silt–clay mixtures derived from the < 425 μm fraction of debris-flow source material. Mixtures contained 50%, 65%, and 80% fines at water contents of 50–60%, corresponding to volumetric solid fraction C_v= 0.386-0.430. All tested mixtures exhibit non-Newtonian behavior with pronounced shear-thinning response. Yield stress determined from Herschel–Bulkley and Bingham model fitting ranges from 6.8 Pa to 133.3 Pa across the tested compositions and concentration interval. Despite the relatively narrow C_v range, yield resistance increases markedly with increasing C_v. Mixtures with lower fines content show greater sensitivity to changes in volumetric solid fraction (C_v), whereas fines-enriched mixtures exhibit more moderate yield variation. These results indicate that both $C_v$and fines proportion control rheological behavior under debris-flow-relevant conditions and provide experimentally constrained parameters for debris-flow mobility analyses.

1 Introduction

Debris-flow mobility is governed by the rheological response of soil–water mixtures, which depends primarily on volumetric solid fraction and particle interactions. Experimental studies demonstrate that yield stress increases strongly with solid concentration and that mechanical transitions may occur within concentration ranges relevant to natural debris flows (Sosio & Crosta[1], Jeong et al.[2]). Despite these findings, laboratory-constrained evaluation of sand–silt–clay mixtures within narrow, field-relevant concentration intervals remains limited.
This study investigates the rheological behavior of fines-enriched sand–silt–clay mixtures derived from the <425 μm fraction of material collected from the collapse area of the 2021 Atami debris flow. Laboratory mixtures containing 50%, 65%, and 80% fines (silt + clay fraction) were prepared at water contents corresponding to solid volume fractions $C_v = 0.386–0.430$. The objective is to quantify shear stress–shear rate behavior, determine yield stress, and evaluate its dependence on solid volume fraction within this concentration range.

2 Materials and Experimental Methods

2.1 Material description

The tested material was collected from the remaining embankment on the southern slope of the 2021 Atami debris flow source valley, which remained intact after the collapse. The particle-size distribution consists of 14.9% (0.425–1 mm), 8.7% (0.25–0.425 mm), 12.7% (0.15–0.25 mm), 6.2% (0.106–0.15 mm), 3.3% (0.075–0.106 mm), and 20.0% fines (<0.075 mm). Including the coarse fraction greater than 1 mm (34.2%), the material contains 45.8% sand (0.075–1 mm) and 20.0% fines (<0.075 mm), with the remaining 34.2% comprising particles larger than 1 mm. The soil index properties are summarized in Table 1.

2.2 Testing procedure

Rheological measurements were conducted using a rotational viscometer (Atago Visco B 695) equipped with a concentric-cylinder system (Table 2). Samples were pre-sheared at 30 rpm to minimize structural history effects (Barnes, 1997), followed by stepwise shear over approximately 1–60 s^{-1} (5–250 rpm). Steady shear stress was recorded at each step, and yield stress was obtained from fitting the shear stress–shear rate data to constitutive models.

Table 1 Index properties of testing material

Property	Index parameter	Value
Specific gravity	G_s	2.62
Atterberg limits	Liquid limit, LL(%)	41
	Plastic limit, PL(%)	30
	Plasticity index, PI(%)	11
Soil Classification (USCS)	ML	

Table 2 Geometrical parameters of measuring system

Parameter	Definition	Value
Gap distance	$\Delta = R_c - R_s$(mm)	7.5
Gap ratio	$\delta = R_c/R_s$	2.9
Radius ratio	$r = 1/\delta$	0.33
Maximum particle size	$d_{max} = \Delta/10$(mm)	0.75

Note: R_c= radius of standard beaker, R_s= radius of spindle.

2.3 Volumetric solid fraction

The volumetric solid fraction $C_v$was determined from measured water content assuming a two-phase soil–water system with incompressible constituents. Water content is defined as $w = M_w/M_s$, where M_w and M_s denote the mass of water and solids, respectively. Using the standard mass–volume relationship and the specific gravity of solids G_s, the volumetric solid fraction is expressed as $C_v = 1/(1 + wG_s)$ with $G_s = 2.62$, the tested water contents of 50–60% correspond to $C_v = 0.430$ (50%), 0.407 (55%), and 0.386 (60%). This range defines the concentration interval investigated in the rheological analysis.

2.4 Shear rate calculation

Shear rate was evaluated using the concentric-cylinder (Couette) formulation appropriate for rotational viscometry. Angular velocity ω was calculated from the rotational speed N(rpm) as $\omega = 2\pi N/60$. For a concentric-cylinder system, with R_s and R_c denoted as the spindle and cup radii, the general shear-rate expression $\dot{\gamma}$, is given as

$$\dot{\gamma} = \frac{2\omega R_c^2}{R_c^2 - R_s^2} \qquad (1)$$

3 Results and Discussion

3.1 Flow curves and Bingham fits

Fig. 1 shows the shear stress–shear rate relationships for the eight mixtures with Bingham fits, where W and F denote water content and fines percentage, respectively. Apparent yield stresses range from 6.3 to 133.3 Pa despite the narrow concentration interval. The Bingham fits yield coefficients of determination of $R^2 =$ 0.77–0.94, indicating that the model provides a reasonable first-order approximation of the observed viscoplastic behavior. Higher R^2 values from power-law fitting (0.91– 0.98) confirm measurable shear-thinning, particularly in fines-enriched mixtures. Within $C_v = 0.386$–0.430, yield stress varies by more than one order of magnitude, with sand-rich mixtures showing stronger concentration sensitivity than fines-enriched mixtures.

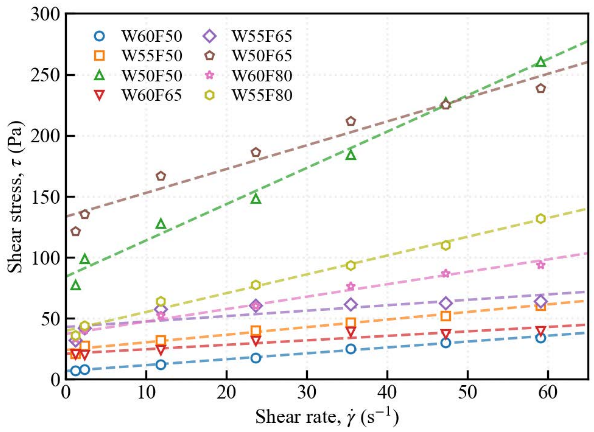

Fig. 1 Shear stress- shear rate relationship with Bingham fitting.

3.2 Stress dependence on volumetric solid fraction

Fig. 2 shows the variation of yield stress with volumetric solid fraction together with the exponential regression fit. A clear exponential dependence is observed, which can be expressed as

$$\tau_y = \alpha \cdot 10^{\beta C_v} \qquad (2)$$

Fitting this relationship to the experimental dataset yields a concentration coefficient of β = 17.8 (R^2 = 0.901), indicating strong sensitivity of yield stress to changes in solid fraction. The magnitude of β implies that a 0.01 increase in C_v results in approximately a 50% increase in yield stress within the tested range. Across $C_v = 0.386$–0.430, yield stress increases from approximately 6 Pa to over 100 Pa, corresponding to more than one order of magnitude variation. This pronounced concentration dependence exceeds values reported for typical clays and soils (β ≈ 7–10; Zarch et al.[4]), suggesting enhanced mechanical sensitivity of the tested material to modest changes in water content. Such concentration sensitivity implies that small changes in water content may substantially modify mixture resistance under field conditions. The July 2021 Atami event was preceded by approximately 589 mm of rainfall (Shizuoka Prefecture, 2021[5]), illustrating how hydrological variation may induce substantial reductions in mechanical resistance.

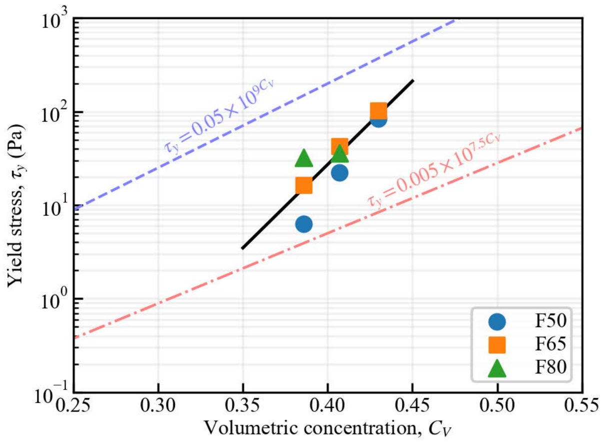

Fig. 2 Yield stress as a function of volumetric solid fraction.

3.3 Apparent viscosity and shear-thinning behavior

Fig. 3 shows the apparent viscosity as a function of shear rate. All mixtures exhibit shear-thinning behavior, with viscosity decreasing systematically as shear rate increases. The greatest separation among mixtures occurs at low shear rates (≤ 5 s^{-1}), where structural resistance dominates and viscosity varies by more than one order of magnitude. At higher shear rates, the curves converge, indicating progressive breakdown of particle networks. Sand-rich mixtures show stronger viscosity amplification with increasing solid fraction, consistent with the yield– C_v trends. This rate-dependent reduction in viscosity implies that assuming constant viscosity may underestimate mobility in debris-flow modeling.

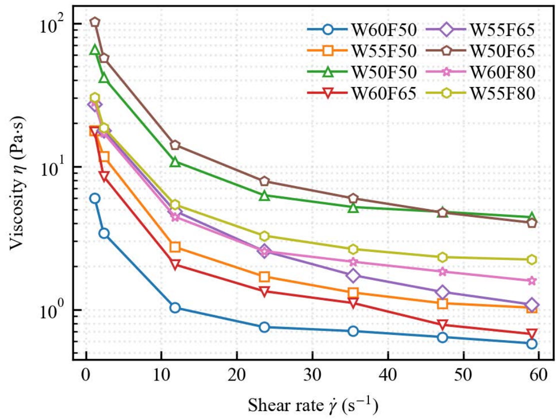

Fig. 3 Apparent viscosity versus shear rate.

4 Conclusions

Rotational rheometry of sand–silt–clay mixtures at water contents of 50–60%, ($C_v = 0.386$–0.430) demonstrates strong concentration dependent viscoplastic behavior. Bingham fitting yields apparent yield stresses of approximately 6–133.3 Pa within this narrow C_v interval. Yield stress increases exponentially with solid volume fraction (β = 17.8, R^2 = 0.901), indicating high mechanical sensitivity to small concentration changes. All mixtures exhibit shear-thinning behavior, with viscosity decreasing systematically with shear rate. Within the tested interval, a 0.01 increase in C_v corresponds to approximately a 1.5-fold increase in yield stress, underscoring exponential sensitivity of resistance. These findings, limited to the investigated concentration range and fines-enriched mixtures, confirm that volumetric concentration is the primary control on matrix resistance and should be explicitly considered in debris-flow rheological modeling.

References

1) Sosio, R., & Crosta, G.B.: Rheology of concentrated granular suspensions and implications for debris flows. Eng. Geol., 109, 81–92, 2009
2) Jeong, S. W., Lee, S., Oh, H.J, et al. Determining the debris flow yield strength of weathered soils: a case study of the Miryang debris flow in the Republic of Korea. Sci Rep 14, 20975, 2024
3) Barnes, H. A.: Thixotropy — a review. J. non-Newton. Fluid Mech., 70, 1–33, 1997
4) Zach, K. M., Zhang, L., Haeri, S. M., and He, J.: Classic, modern, and physics-based rheological laws for geophysical granular flows in landslide hazard chain. Earth-Science Reviews, 269, 105204, 2025
5) Shizuoka Prefecture. Geotechnical Investigation Results (Preliminary Report) on the Atami City Izusan District Debris Flow. River and Sabo Bureau, Shizuoka, Japan, 2021.